Experimental investigation and 1D analytical approach on convective heat transfers in engine exhaust-type turbulent pulsating flows

Marco Simonetti, Christian Caillol, Pascal Higelin, Clément Dumand, Emmanuel Revol

Experimental Investigation and 1D Analytical Approach on Convective Heat Transfers in Engine Exhaust-Type Turbulent Pulsating Flows

Marco Simonetti[a,*], Christian Caillol[a], Pascal Higelin[a], Clément Dumand[b], Emmanuel Revol[b]
[a]Laboratoire PRISME, Université d'Orléans, 8 rue Léonard de Vinci, 45072 Orléans Cedex 2, France
[b]Groupe PSA, Route de Gizy, Vélizy-Villacoublay, France
*Corresponding author, E-mail address: ms.marco.simonetti@gmail.com

Abstract

In many practical engineering situations, such as in the exhaust pipes of Internal Combustion Engines, heat is transferred under conditions of pulsating flow. In these conditions, the heat transfer mechanism is affected by the pulsating flow parameters. The objective of the present work was to experimentally investigate heat transfers for pulsating turbulent pipe flows with large-amplitude oscillations. A specific experimental apparatus able to reproduce a pulsating flow representative of the engine exhaust was designed. A stationary turbulent hot air flow with a Reynolds number of 30000, based on the time average velocity, is excited through a pulsating mechanism and exchanges thermal energy with a water cooled steel pipe. Pulsation frequency ranged from 10 to 95 Hz. An analytical formulation, derived from the 1D energy balance equation for a turbulent pulsating flow, and an ad-hoc experimental procedure evidenced that, in the case of a reversed pulsating flow, a contribution to the energy balance equation through the boundaries, which impacts the total convective heat transfers, may occur. It was also observed that the flow pulsation enhances heat transfers in the entire range of the investigated frequencies. In particular, the results show that when the flow is excited with a frequency equal to a resonance mode of the system, a strong increase in heat transfers occurs. Instantaneous measurements of air velocity and temperature demonstrated that the increase in the energy axial advection due to the oscillating component of the velocity is the major cause of the heat transfer enhancement. The relative Nusselt number was found to be directly linked to the ratio between the velocity oscillation amplitude and the time-average component of the axial bulk velocity, suggesting that this characteristic term is representative of the predominant heat transfer enhancement mechanism.

Keywords: *Heat transfer enhancement, Turbulent pulsating flow, 1D analytical analysis, Experimental investigation, Internal combustion engines.*
Declarations of interest: *none*

Highlights

- Convective heat transfers for pulsating turbulent pipe flows are investigated.
- The impact of the pulsation frequency on heat transfers is studied.
- A heat transfer enhancement in the case of a flow in resonant conditions is observed and analyzed.
- Increased Nusselt number is linked to the amplitude of the velocity waveform.

Nomenclature

Roman letters

c	velocity of sound
c_p	constant pressure specific heat
D	diameter
f	pulsation frequency
Gz_T	Graetz number
h_{air}	convective heat transfer coefficient of air
h_{water}	convective heat transfer coefficient of water
L	length of the pipe
L_d	thermal entrance length
Nu	Nusselt number
Nu_{rel}	relative Nusselt number
p	pressure
Pr	Prandtl number
q	specific convective heat transfer
Q_{conv}	total convective heat transfer
R_{in}	internal radius
R_{out}	external radius
Re	Reynolds number
S	exchange surface
T	temperature
$T_{b,in}$	inlet bulk temperature of air
$T_{b,out}$	outlet bulk temperature of air
$T_{centerline}$	air temperature at the pipe centerline
$T_{H2O\text{-}in}$	inlet temperature of water
$T_{H2O\text{-}out}$	outlet temperature of water
ΔT_{lm}	logarithmic temperature difference
u	local axial velocity
$u_{centerline}$	axial velocity at the pipe centerline
$\bar{u}$	time-average component of the axial bulk velocity
$\Delta< u >$	phase-averaged bulk velocity oscillation amplitude
U_0	Lagrangian velocity
V	volume
Wo	Womersley number
Z	local instantaneous property of the flow
$\bar{Z}$	time-average component of the flow property
$\tilde{Z}$	oscillating component of the flow property
Z'	turbulent component of the flow property

Greek symbols

λ_{wall}	thermal conductivity of the pipe wall
λ	thermal conductivity of air
ρ	air density
δ	velocity boundary layer
μ	air dynamic viscosity
ω	pulsation of the flow

1. INTRODUCTION

The term '*pulsating*' or '*pulsatile*' is usually used to describe a flow field composed of a steady and an oscillating part which is cyclically repeated in time. This kind of flow is encountered in a wide range of physical systems and engineering applications such as the intake and exhaust manifolds of internal combustion engines. As observed by Host et al. [1], because of the ever stricter emission standards imposed by governments, particular attention has been paid to the design of the exhaust and intake manifolds. A good management of heat losses, in which the heat transfer process in pulsating flow conditions plays a major role, is an important requirement for after-treatment systems control and optimization. Considering the exergetic limits, waste energy recovery (WER) represents a promising way to go further in fuel saving and pollutant emissions control. Several technologies for WER have been extensively investigated in the past few years, each of these systems extracts the thermal energy still available in the engine exhaust gases and converts this energy in mechanical or electrical output. For instance, in a review on the use of the Rankine cycle for Internal Combustion Engines exhaust waste heat recovery, Sprouse et al. [2] have reported a potential fuel economy of around 10%. In a Rankine machine, improving the heat exchanger efficiency by convection process enhancement is a key that can potentially lead to compact and economic heat exchangers. Although for a stationary flow the Reynolds number characterizes the laminar or turbulent behavior of the bulk flow, the amplitude and the frequency of the superimposed oscillations play a dominant role in the structures of the pulsating flow. Over the past decades, many studies have been dedicated to pulsating flows and their associated heat transfer process, in a wide range of experimental configurations. However, some of the available results are contradictory and the main question is still open: *does pulsation enhance, or degrade, heat transfers compared to a steady flow*?

In a first study, Dec et al. [3] studied the influence of pulsation frequency, amplitude and mean flow rate on the heat transfers for a pulse combustor tail pipe. Pulsation frequency was varied from 67 to 100 Hz, for a Reynolds number based on the time average velocity varying between 3100 and 4750. Spatially averaged Nusselt numbers were observed to increase linearly with both pulsation frequency and amplitude, while the Nusselt number enhancement decreased with increasing mass flow rate despite accompanying increases in oscillation frequency and amplitude. Cycle-resolved Nusselt number results, discussed in a second study by Dec et al. [4], showed that the Nusselt number was nearly constant throughout the cycle, with the exception of local increases at flow reversal times. Several mechanisms responsible for the heat transfer enhancement in oscillating flows were reviewed and discussed. Among these, acoustic streaming, which corresponds to the appearance of a secondary time-averaged velocity component having the form of large longitudinal recirculation cells, and entrance length effects were considered to have a slight influence on the observed Nusselt number enhancement. Detailed studies of time-resolved velocity and temperature fields [5,6] showed that the heat transfer enhancement was most likely caused by a combination of increased turbulent intensity and strong transverse flows generated during the streamwise velocity reversals.

Xu et al. [7] studied the flow properties of a self-excited Helmholtz pulse combustor elbow tailpipe. The results showed that, due to pulsation and flow reversal, Dean Vortex forming, shedding and reforming processes periodically contribute to convective heat transfer enhancement. With the same type of experimental apparatus, Zhai et al. [8] proposed a Nusselt correlation for the pulsating flow, based on the addition of two independent physical properties. Applying the quasi-steady theory and the Vaschy-Buckingham theorem to the convection heat transfer problem, the ratio between the velocity amplitude and the time-averaged velocity and the ratio between the pulsation velocity scale and the time-averaged velocity were found to be the aforementioned independent physical properties. Several studies were also conducted on turbulent and laminar pulsating pipe flows. In the work of Patel et al. [9], the Reynolds number ranged from 7000 to 16500, while the pulsation frequency was varied from 1 Hz to 3.33 Hz. Results showed that the Nusselt number was strongly affected by both pulsation frequency and Reynolds number with a 44.4% maximum enhancement of the heat transfer coefficient at the pulsation frequency of 3.33 Hz. In a study on a pulsating turbulent water stream, Zohir [10] also pointed out that the heat transfer coefficient was strongly affected by pulsation frequency and amplitude and by the Reynolds number. The improvement in heat transfers was attributed to an increased level of turbulence and the introduction of forced convection in the boundary layer. The experimental studies by Said et al. [11] and Nishandar et al. [12] confirmed that the heat transfer coefficient was either increased or decreased as a function of the pulsation frequency in turbulent conditions. Elshafei et al. [13] conducted a numerical study of the heat transfers for a fully developed pulsating turbulent flow over a range of $10^4 \leq Re \leq 4 \cdot 10^4$ and $0 \leq f \leq 70$ Hz and the results were compared with the available experimental data. Results showed a slight reduction in the time-averaged Nusselt number with respect to that of a steady flow. However, in the fully developed established region, the local Nusselt number was either increased or decreased, compared to Nu values for steady flow, depending on the frequency parameter. In recent studies, flow pulsation was also investigated as an active method to enhance heat transfers in industrial

applications such as heat exchangers. Kharvani et al. [14] investigated the potential to increase heat transfers by using a rotating ball valve as a pulse generator mounted downstream/upstream of a spiral-coil tube. The Reynolds number ranged from 6220 to 16300, while the pulsation frequency was varied from 0 to 20 Hz. It was observed that, although the overall average heat transfer coefficient was strongly affected by the Reynolds number, it was enhanced by up to 26% for a pulsating flow compared to a steady flow. Ghaedamini et al. [15] investigated the potential to increase heat transfers with wavy walled micro-channels. Although such geometries demonstrated their capability of inducing chaotic advection, a substantial pressure drop penalty was observed for highly modulated channels. To overcome this issue, a pulsating flow was introduced, leading to a strong enhancement of heat transfers for channels with slightly modulated walls corresponding to a reasonable pressure drop penalty. This increase was attributed to a chaotic advection phenomenon near a characteristic excitation frequency. In [16], Wantha experimentally studied the enhancement of heat transfer in finned tube heat exchangers by using a pulsating air flow. The influence of velocity amplitude, pulsation frequency, Reynolds number and blockage ratio of heat exchangers was investigated. The results showed that the pulsation frequency and velocity amplitude play major roles in heat transfers. An empirical correlation, based on a Colburn j-factor, was deduced from the experimental results.

Several attempts were also made to generalize Nusselt number correlations to pulsating flows in a pipe. Guo et al. [17] numerically tested various forms of the Nusselt number correlation and proposed an improved version describing, on the one hand, a high heat transfer enhancement for a large amplitude pulsation flowrate, and on the other hand both heat transfer enhancement and reduction, depending on the pulsation frequency, for a small amplitude pulsation. As reported by the aforementioned surveys, it has been frequently observed that pulsation frequency may have an impact on the convective heat transfers. However, the variety of the experimental configurations and the variety of the pulsation creation mechanisms have led to some controversies: both enhancement and degradation of convective heat transfers have been observed. Besides, the main physical mechanisms involved have not been fully described.

In the present study, an experimental investigation was conducted on heat transfer phenomena for a pulsating turbulent pipe flow, in a wide range of variation of the physical parameters. The main purposes were to investigate the impact of the pulsation frequency on heat transfers and to identify the main physical mechanisms involved in the heat transfer modification. The design of an experimental apparatus, able to reproduce a pulsating pipe hot air flow over a range of $10 \leq f \leq 95$ Hz and $10^4 \leq Re \leq 5 \cdot 10^4$, representative of engine exhaust flow operating conditions, is presented. In the test-rig, the pulsating hot air flow exchanges thermal energy with cold water flowing in the opposite direction. The work presented in this paper focuses on the time- and space-averaged characterization of the convective heat transfers. Experimental results are linked to the 1D energy balance equation of the pulsating turbulent pipe flow to identify the characteristic terms representative of the heat transfer modification due to the pulsating conditions. In order to enhance the predictive capability of engine numerical tools, these terms could be included in convective coefficient correlations, to take into account flow velocity fluctuations, instead of using empirically calibrated corrective parameters as in models recently developed [18] to compute the gas

temperature drop along the exhaust runner and manifold. The 1D approach is adopted in the present work to be consistent with engine simulation codes commonly used when accurate modeling of heat transfers in exhaust systems is required [19]. Data collection and reduction are presented; results in terms of a relative Nusselt number are reported and discussed based on this assumption.

2. Analytical Formulation of the Problem

The effect of the pulsation on heat transfers can be characterized in terms of the relative Nusselt number Nu_{rel}, defined as the ratio of the time-averaged Nusselt number for the pulsating flow to the corresponding one for a steady flow with the same time-averaged Reynolds number. For an air flow into a cylindrical control volume, the time-averaged Nusselt number is defined as in the following equation:

$$Nu = \frac{h_{air}\, D}{\lambda} = \frac{Q_{conv}\, D}{S\, \Delta T_{lm}\, \lambda} \tag{1}$$

where Q_{conv} is the time-averaged convective heat transfer, D the internal diameter of the pipe, S the exchange surface, ΔT_{lm} the logarithmic mean temperature difference between the air and the internal wall of the pipe and λ the thermal conductivity of air. The relative Nusselt number definition has been adopted in several previous studies because of its ability to bring out the impact of the pulsation frequency on heat transfers and to identify a corrective coefficient for a Nusselt correlation accounting for pulsating effects. The practical difficulty in such an approach consists in correctly assessing the time-averaged convective heat transfer Q_{conv}. Since in some applications the measurement of the heat flux exchanged with a solid wall is difficult to achieve, Q_{conv} is computed starting from the air flow properties by solving the energy balance equation. The time-averaged convective heat transfer is generally computed from the variation of the time-averaged component of the air enthalpy through the inlet and outlet sections of the control volume, but it is shown in the following development that this calculation does not take into account characteristic terms related to the pulsating component of the flow. In the present work, Q_{conv} is derived from the time-averaged and space-integrated form of the instantaneous energy balance equation for a pulsating turbulent pipe flow. The terms related to the heat flux propagated from the advection of the oscillating component of the flow are highlighted.

Assuming negligible viscous dissipation, the 2D instantaneous local energy balance equation in cylindrical coordinates, for an incompressible pipe flow with constant fluid properties, exhibits the following form:

$$\rho c_p \left(\frac{\partial T}{\partial t} + \frac{\partial (uT)}{\partial x} + \frac{\partial (vT)}{\partial r} \right) = \lambda \left(\frac{\partial^2 T}{\partial x^2} + \frac{1}{r} \frac{\partial}{\partial r} \left(r \frac{\partial T}{\partial r} \right) \right) \tag{2}$$

where u and v represent respectively the axial and the radial instantaneous air velocity components, T the temperature of air, ρ the fluid density and c_p the specific heat at constant pressure. As proposed by Reynolds et al. [20], in the specific case of a turbulent pulsating flow, each of the flow properties can be decomposed into three different terms, as expressed in the following equation:

$$Z(x,r,t) = \bar{Z}(x,r) + \tilde{Z}(x,r,t) + Z'(x,r,t) \quad (3)$$

where $\bar{Z}(x,r)$ represents the time-averaged component, $\tilde{Z}(x,r,t)$ is the oscillating term of the coherent cycle-stationary pattern and $Z'(x,r,t)$ corresponds to the turbulent fluctuations term. Time averaging $\left(\bar{}\right)$ determines $\bar{Z}(x,r)$ and the phase-average $(<>)$, i.e. the average over a large ensemble of points having the same phase with respect to a reference oscillator, leads to:

$$< Z(x,r,t) >= \bar{Z}(x,r) + \tilde{Z}(x,r,t) \quad (4)$$

Phase-averaging removes the background turbulence and extracts only the organized motions from the total instantaneous profile. For the sake of brevity, some useful mathematical properties that follow from the basic definitions of the time and phase averages are not reported here, they are detailed in [20]. Applying successively the phase averaging and then the time averaging operators to Eq. 2, in which the triple decomposition is introduced, leads to:

$$\rho c_p \left(\frac{\partial(\bar{u}\bar{T})}{\partial x} + \frac{\partial\left(\overline{\tilde{u}\tilde{T}}\right)}{\partial x} + \frac{\partial \overline{< u'T' >}}{\partial x} + \frac{\partial(\bar{v}\bar{T})}{\partial r} + \frac{\partial\left(\overline{\tilde{v}\tilde{T}}\right)}{\partial r} + \frac{\partial \overline{< v'T' >}}{\partial r} \right) = \lambda \left(\frac{\partial^2 \bar{T}}{\partial x^2} + \frac{1}{r}\frac{\partial}{\partial r}\left(r \frac{\partial \bar{T}}{\partial r} \right) \right) \quad (5)$$

The left-hand side of Eq. 5 represents the energy transport by mean flow, oscillating motion and fluctuating motion, through the control volume, due to axial and radial advection. The right-hand side of the equation describes the heat conduction, through the control volume, in axial and radial directions. To identify the characteristic terms, in a 1D approach, representative of the impact of the oscillating motion on heat transfers, Eq. 5 is integrated over the cross section of the pipe Σ. Assuming an axisymmetric flow, the cross section integration operator is defined as:

$$\{\cdot\}_\Sigma = 2\pi \int_0^{R_{in}} (\cdot)\, r\, dr \quad (6)$$

where R_{in} is the pipe internal radius. The radial advection terms in Eq. 5 are integrated by parts and, by considering a condition of no-permeability at the wall, it is shown that they are all equal to zero. The radial conduction term is integrated as follows:

$$2\pi\, \lambda \int_0^{R_{in}} \frac{\partial}{\partial r}\left(r \frac{\partial \bar{T}}{\partial r} \right) dr = 2\pi\, R_{in}\, \lambda \left. \frac{\partial \bar{T}}{\partial r} \right|_{wall} \quad (7)$$

The heat flux boundary condition corresponds to heat convection at the wall surface:

$$2\pi\, R_{in}\, \lambda \left. \frac{\partial \bar{T}}{\partial r} \right|_{wall} = \overline{< q(x,t) >} \quad (8)$$

where $q(x,t)$ is the local specific convective heat transfer per unit length ∂x. Considering that axial diffusive transport is negligible compared to the advective transport of energy, the 1D local energy balance equation becomes:

$$\rho c_p \left(\frac{\partial \{\bar{u}\bar{T}\}_\Sigma}{\partial x} + \frac{\partial \{\overline{\tilde{u}\tilde{T}}\}_\Sigma}{\partial x} + \frac{\partial \{\overline{< (u'T') >}\}_\Sigma}{\partial x} \right) = \overline{< q >} \quad (9)$$

By integrating Eq. 9 over the total length L of the pipe (corresponding to the control volume, between the inlet and outlet measuring sections, in the following), the energy conservation equation is written as:

$$\rho c_p \left(\underbrace{\{\bar{u}\bar{T}\}_{\Sigma}\Big|_0^L}_{A} + \underbrace{\{\widetilde{\tilde{u}\tilde{T}}\}_{\Sigma}\Big|_0^L}_{B} + \underbrace{\{\overline{< u'T' >}\}_{\Sigma}\Big|_0^L}_{C} \right) = Q_{conv} \tag{10}$$

The total time-averaged convective heat transfer Q_{conv} is equal to the sum of three different terms: the term *A* which physically represents the energy variation of the time-mean component of the flow across the pipe, the term *B* which represents the energy variation due to the oscillating component of the flow and the term *C* corresponding to the advective transport of energy by fluctuating motion due to turbulence fluctuations. The statement of Eq. 10 clarifies that, whenever a direct measurement of Q_{conv} is not available, instantaneous measurements of the air velocity and temperature are required to correctly compute all the terms in the left-hand side of Eq. 10. In this study, a water flow was used to cool the external surface of the pipe. In addition to keeping the wall temperature cold, constant and quite homogeneous in the pipe section where heat transfers are characterized, this experimental setup allows Q_{conv} to be evaluated directly from the water temperature measurements. In this manner, it is possible to avoid performing instantaneous measurements of the flow properties at the inlet and the outlet of the test-section.

3. Experimental Setup and Procedures

3.1. Experimental Setup

A schematic diagram of the pulsating flow facility is depicted in Fig. 1. It comprises three main parts: the first one produces a hot stationary air flow, the second one transforms the stationary flow to a pulsating flow, and in the last part, in which the flow develops, heat transfers are estimated. In the first part of the test rig, the dry compressed air mass flow rate is measured and regulated by a Brooks SLA5853S {1}, a thermal effect mass flow meter with a maximum flow rate of 2500 Nl/min and with a calibration uncertainty of 0.73% of full scale. Then, air is heated by three Sylvania inline air heaters {3} with a total electric power of 12 kW, ensuring a maximum air temperature of 400°C at the maximum mass flow rate. Hot flow is finally stored in a 30-litre steel tank {4} designed to withstand a maximum air pressure of 10 bar and to dampen the flow pulsation coming back from the pulse generator. Once the hot air flow has been generated it is forced to pass through the pulsating mechanism {5-7}: a mono-cylinder head was chosen to produce a pulsating flow with a maximum frequency of 95 Hz, equipped with a classical pushrod valve train entrained by an electric engine with a power of 3 kW and a nominal velocity of 3000 rpm. In detail, hot air flows from the bottom of the cylinder head and only one of the two intake valves is alternately closed and opened to create the pulsating flow. The intake valve was chosen because of its higher diameter. Air leakages in the cylinder head were experimentally estimated to be below 0.5 kg/h, leading to an error on the mass flow rate measurement of <1%. In order to determine the camshaft position and rotation velocity, an encoder with a resolution of 0.1° is placed on the camshaft. Once the pulsating flow is generated, it is forced to pass through a steel pipe {8-10} in which it develops and exchanges thermal energy. Finally, at the end of the pipe, a 6-litre tank {11} is placed to muffle pressure pulsations. The entire flow facility is then linked to the exhaust line of the laboratory. As shown in Fig. 1, the steel pipe, with an internal diameter of 57.76 mm, is

composed of three different sections: the first one, called *developing section* {8}, has a length of 2.65 meters and a pipe length/internal diameter ratio of 48.4. It was designed to be long enough to completely develop the velocity flow field in the case of a steady turbulent flow. The pipe is thermally insulated to avoid high heat energy losses. The test section {9} (detailed in Fig. 2), with a length of 1 meter, is placed at the outlet of the developing section and is designed to be able to characterize heat transfers.

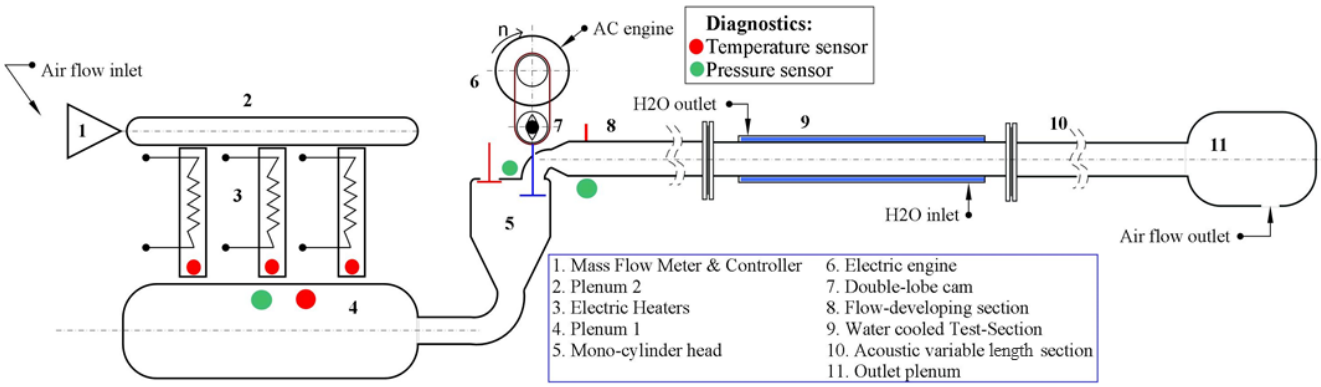

Figure 1: Scheme of the experimental apparatus

The test section consists of a double-wall pipe, in which the pulsating air and cold water flow in opposite directions, respectively in the internal and external parts of the pipe. Water cooling has the advantage of making it possible to manage the wall temperature and of having a homogeneous temperature field in the internal wall of the pipe. Inlet and outlet water temperatures are measured by two 0.5 mm sheathed K-type thermocouples for each section in order to evaluate the total time-averaged convective heat transfer Q_{conv} (see Eq. 10). The two thermocouples by section enable to control the homogeneity of the temperature field and allow to be confident in the temperature measurement at each section. A Kistler Type 2621F conditioning unit, with a maximum cooling power up to 1500 Watt, is used to provide a maximum water flow rate of 6.1 L/min. As shown in Fig. 2, at a distance from the beginning of the test-section of 10 times the internal pipe diameter, several sensors are placed to measure the air velocity, temperature and pressure. In particular, in order to calculate the air bulk temperature, which corresponds to the integral of temperature on the cross section, in the first measuring section (A – A' in Fig. 2) four sheathed K-type thermocouples with a 0.5 mm diameter are placed at different distances from the wall, respectively 1, 0.5, 0.125 and 0.0625 times the pipe radius. Furthermore, a Kulite pressure transducer is placed to measure the instantaneous static pressure of air. The same measuring configuration was used for the outlet section of the test-section. For the remaining sections, except the section B – B', only one 0.5 mm sheathed K-type thermocouple is placed at the centerline of the pipe.

The thermocouples protrusion lengths have been chosen to compute accurately the bulk air temperature. The choice of the number and position of the thermocouples was based on the minimum number required to describe a presumed temperature radial profile. As, for a pulsating flow, a theoretical temperature profile is unknown, the temperature radial profile for a stationary turbulent pipe flow, developped by Johnk et al. [21] and described by Eq. 11, has been adopted:

$$\frac{(T_w - T)}{(T_w - T_{centerline})} = (1+s)\left(\frac{y}{R_{in}}\right)^{1/m} - s\left(\frac{y}{R_{in}}\right)^{(1+s)/sm} \quad (11)$$

where T_w is the wall temperature, $T_{centerline}$ is the temperature at the pipe centerline, y is the distance from the pipe centerline, $s = 0.02$ for all Reynolds numbers, m is function of the Reynolds number and is equal to 5.7 for a Reynolds number of 30000. From Eq. 8, it can be shown that, for the pipe radial interval ranging from $y/R_{in} = 0.1$ to the pipe centerline, the polynomial which approximates the temperature profile with the higher coefficient of determination is a 3rd order polynomial. Consequently, four temperature measurements were chosen since they correspond to the minimum number of values required to determine a 3rd order polynomial.

In the section B – B', in addition to a Kulite pressure transducer, a Constant Temperature Anemometer and two unsheathed micro-thermocouples are placed to measure the instantaneous radial profiles of air velocity and temperature. In particular, a Dantec 55P71 double wire probe (*HWA* in Fig. 2) was used to measure the air velocity magnitude and direction. The phase-averaged wire voltage was corrected to account for air temperature variations, and the flow reversal was detected thanks to the spatial orientation of the wire probe. When placed parallel to the flow direction, this probe is widely used to measure the spatial gradient of the flow velocity in wind tunnel application. In this study, it has been placed perpendicular to the flow in order to make possible the detection of the velocity direction by comparing the voltage signals of the two parallel wires, outdistanced of 0.4 mm. Because of the distance between the wires, flow reversal event, corresponding to the minimum of the wire voltage signal, shows a phase delay when the wire signals are compared. The wire that firstly senses the flow reversal has a phase of the minimum of the signal advanced in comparison to the other wire. Once the flow reversal is detected, the velocity is computed only from the first wire in the flow direction. Furthermore, a higher standard deviation of the phase-averaged velocity of one wire in comparison to the other one, resulting from the perturbations created by the first wire on the second one, was used as a second method to validate the detection of the flow direction.

The energy balance equation applied to the hot junction of a thermocouple describes the temperature difference between the gas and the hot junction with a thermocouple temperature delay due to the finite mass of the hot junction and due to the convective heat transfer between the fluid and the thermocouple. Assuming negligible thermal conduction and radiation in this equation, the hot junction temperature can be modelled as a first-order system, where the time constant represents the time the sensor requires to reach the gas temperature. For rapid temperature measurements, the time constant has to be compared to the dynamic of the flow properties variation in order to know if a compensation of the time delay has to be applied to the thermocouple signal to compute the real fluid temperature. A Kalman Filter method [22] was applied to the signal of the two micro-thermocouples (*T1-kf, T2-kf* in Fig. 2) to calculate in-situ the time constant of the sensor in order to correct the raw thermocouple measurements and to estimate the actual air temperature. The method was experimentally validated using a reference temperature signal measured with a cold wire with a diameter of 1 µm which has a frequency bandwidth up to 1 kHz. The employed micro-thermocouples had a diameter respectively of 25 µm and 50 µm. An ad-hoc experimental characterization of the thermocouple had shown that for an unsheathed micro-thermocouple with a diameter of 25 µm the

sensor time-constant ranges from 25 msec to 10 msec for a flow velocity respectively of 2 m/s and 60 m/s, which is in agreement with the results of Tagawa et al. [23]. It was also observed that the time-constant evolution in function of the air velocity follows a logarithmic trend. An uncertainty less than 3% was found. The *HWA* and the micro-thermocouples are connected to the pipe with a concentric screw system with a thread pitch of 1 mm.

As shown in Fig. 1, downstream the test-section, a pipe with a variable length was used. The total length of the pipe can vary from 3.61 meters to 5.91 meters. A NI-9035 cRIO and the LabView software were used to control all the devices in the experimental apparatus and to acquire data.

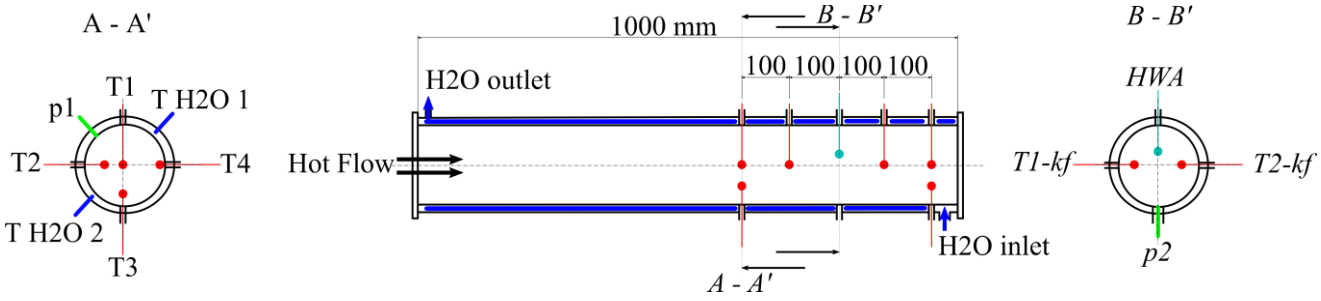

Figure 2: Test-section

3.2. Procedure

The study of the impact of the flow pulsation on heat transfer phenomena was achieved by exciting a steady hot air flow with a pulsation frequency ranging from 0 to 95 Hz. The minimum attainable frequency is 10 Hz, for lower frequencies the electric motor is unable to perform constant speed revolution. A time-averaged mass flow rate of 110 kg/h is forced to flow through the mono-cylinder head. The centerline air temperature at the inlet of the test-section is maintained constant at 150°C for all experiments by regulating the electric power of the air heaters with a PID controller. These flow conditions correspond to a time-averaged Reynolds number of 30000, corresponding to turbulent flow conditions. The cooling water temperature at the inlet of the test-section is kept constant at 17.4°C for each experiment, with a maximum test-by-test variation of around 0.2°C. Accounting for the limitations of the hydraulic circuit used to cool the test-section and given the water mass flow rate, 17.4°C was the lowest achievable and repeatable temperature in order to maximize heat transfers from the hot air to the cold water to reach large temperature variations. The instantaneous mass flow rate profile imposed on the flow, in this manner, is dependent on the flow pulsation frequency and the pipe acoustic responses. This means that while the time-averaged component of the mass flow rate is kept constant for all the flow pulsations, the oscillating component is not constant. In order to extract coherent phenomena responsible for the convective heat transfer mechanisms, three different pipe lengths were investigated (3.69, 4.69 and 5.91 meters). In this manner both the flow pulsation frequency and the acoustic resonance modes of the pipe were varied, making it possible to study the influence of one characteristic on the other. To characterize the acoustic resonance modes of the test-rig pipe for all the different lengths, a further experiment was conducted: after thermal stabilization of the experimental apparatus, by generating a steady hot air flow with an air temperature of 150°C at the inlet of the test section, the system was

subjected to a pressure impulse and then allowed to resonate. Instantaneous pressures were measured at four different axial positions along the pipe and analyzed to compute the resonance mode frequencies of the system.

4. RESULTS AND DISCUSSION

4.1. Acoustic characterization of the pipe

When the experimental apparatus is excited with a rapid mass injection, a pressure wave travelling the pipe is produced. By measuring the instantaneous air static pressure inside the pipe, it is possible to compute the acoustic resonance modes of the system. The rapid mass injection was created by compressing the air inside the cylinder head and by opening the cylinder head valve only one time during one pulsation cycle. The acoustic resonance frequencies were determined by computing the power spectral density (PSD) of the pressure signal, which describes the distribution of power into frequency components. These resonance frequencies correspond to the local maxima of the PSD. In this study, a second order low-pass filter with a cut-off frequency of 1 kHz was applied to the sensor signals before calculating the PSD. Sensor signals were acquired at a frequency of 20 kHz, high enough to respect the Nyquist-Shannon sampling theorem. Because the behavior of the pressure response to a mass injection is qualitatively the same for each pipe length, in the following figures only the pressure signal for one pipe length is shown. Fig. 3 shows the instantaneous pressure, measured at the center of the test-section, and Fig. 4 shows the PSD of the signal obtained for a specific pipe length. The other pressures, measured at different pipe axial positions or for the other pipe lengths, show the same PSD results and are not reported here. Local maxima of the PSD are identified by the red points on Fig. 4. Table 1 shows the first six calculated resonance frequencies for the three tested pipe lengths. They result from the same resonance phenomenon occurring in the pressure field when the pulsation source reaches a pulsation frequency equal to one of the acoustic characteristic frequency of the system. Results show that the first resonance mode of the system is quite different from the resonance frequency calculated for a pipe closed at one end and open to the surrounding air at the other end, which is equal to $f_r = nc/4L$, where n is a natural integer number equal to 1 for the first resonance mode, c is the speed of sound and L is the pipe length. This means that the volume of the outlet plenum is not large enough to be representative of an open exhaust at pressure and temperature ambient conditions. This implies that a detailed numerical modeling of the experimental apparatus should take into account this result through the description of the boundary conditions.

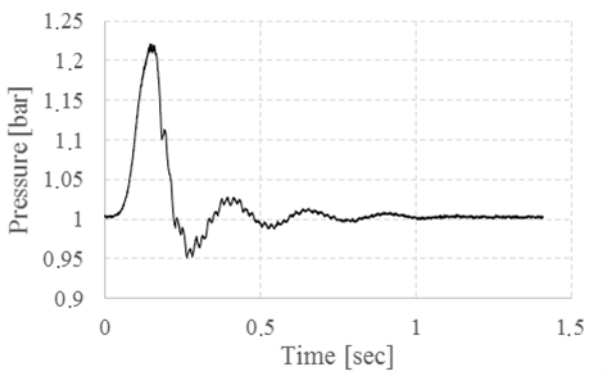

Figure 3: Instantaneous pressure, L = 5.91m

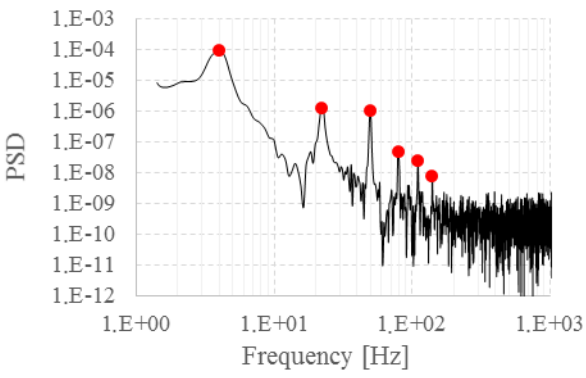

Figure 4: Power Spectral Density, L = 5.91m

Resonance Mode	1	2	3	4	5	6
Resonance Frequency [Hz] **L = 3.69m**	6.4	36.1	79.6	126.3	176.2	239.8
Resonance Frequency [Hz] **L = 4.69m**	4.7	26.2	63.1	101.3	138.9	175.8
Resonance Frequency [Hz] **L = 5.91m**	3.9	22.2	49.5	80.5	110	139.8

Table 1: Resonance frequencies [Hz] of the test-bench for different pipe lengths

4.2. Validation of measurements procedure: steady state operation and boundary conditions

Given the difficulty of measuring the three terms in the left-hand side of Eq. 10 experimentally, the total time-averaged convective heat transfer Q_{conv} was evaluated from the water temperature measurements. In practice, a constant water volumetric flow rate of 4.74 L/min is forced to pass through an annular section, with an internal diameter of 67.3 mm and a thickness of 7 mm, in order to cool the pipe wall. In these operating conditions, the Reynolds number of the water flow is 788, leading to a laminar velocity profile under steady state conditions. Consequently, from the energy balance equation for the water, in which the convective heat transfer with the exterior ambient air was estimated to be less than 10 W and was therefore neglected, Q_{conv} can be solved as the time-averaged enthalpy difference of the water between the inlet and the outlet of the test-section. The computed Q_{conv} and the term A of Eq. 10 are plotted in Fig. 5 and Fig. 6 as a function of the pulsation frequency. It should be noted that pressure pulsation amplitude varies with the frequency (which is illustrated in Figs. 8 and 9 for two different pulsation frequencies). Uncertainties are depicted by error bars. The total uncertainty on convective heat transfers evaluation was determined by applying the error propagation methodology on the energy balance equation for the water flow: $\Delta Q_{conv}/Q_{conv} = \Delta\dot{m}_{H2O}/\dot{m}_{H2O} + \Delta(\Delta T_{H2O})/\Delta T_{H2O}$ where $\dot{m}_{H2O}$ is the water mass flow rate and ΔT_{H2O} is the temperature difference between the inlet and outlet water temperatures. The relative uncertainty for Q_{conv} due to the mass flow rate measurement was 3% for all the pulsation frequencies. To evaluate the relative uncertainty due to the measurement of the water temperature difference, the experimental standard deviation of this temperature difference has been determined based on a set of ten tests for each frequency. From the instantaneous temperature measurements corresponding to an acquisition period of 2 minutes (the data rate was fixed at 10 Hz), the instantaneous inlet and outlet water temperatures were computed by averaging the two thermocouples measurement for each section. The instantaneous inlet/outlet temperature difference was then computed. From this temporal profile, the time-averaged value and the standard deviation were calculated for each test.

Finally, the mean temperature difference was obtained by averaging the ten time-averaged temperature difference and the standard deviation was taken as the largest standard deviation obtained for the set of ten tests.

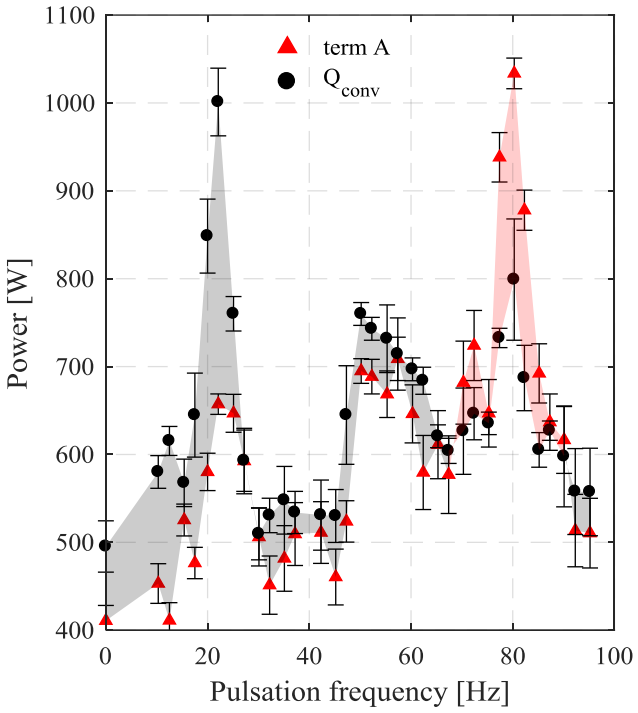

Figure 5: Energy balance equation terms, w/o dry ice, L = 5.91m

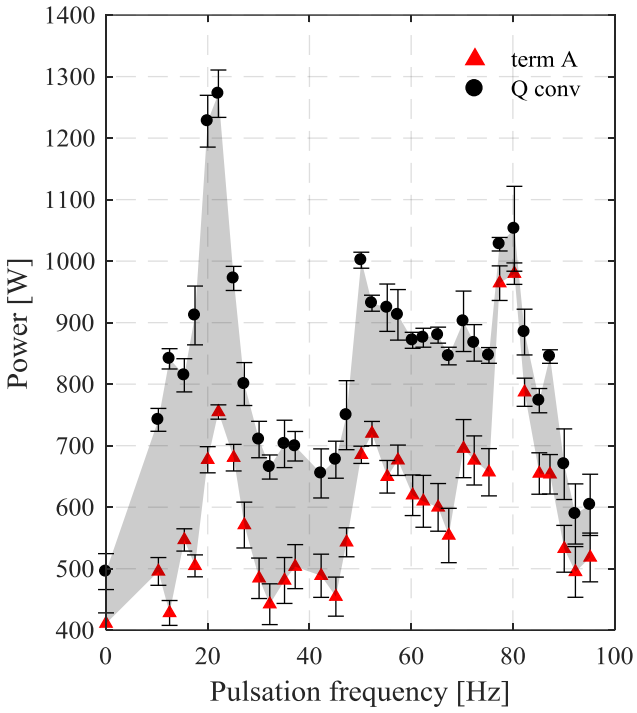

Figure 6: Energy balance equation terms, w/ dry ice, L = 5.91m

The air steady turbulent state (for the particular case with a time-averaged Reynolds number of 30000) is taken as the reference case. In such particular conditions, the term *B* in Eq. 10 is null, making it possible to compare Q_{conv} computed from experiments to the theoretical predicted one. The Nusselt number was evaluated using the Colburn and the Dittus-Boelter correlations and applying the Bhatti and Shah corrective coefficient [24] to take entry effects into account. For a *Re* of 30000, the space-averaged Nusselt number was found to be equal to 89.4 with the Colburn correlation and 92 with the Dittus-Boelter correlation. The total convective heat transfer linked to the Colburn correlation is 482 W, which corresponds to a difference of 2.7% with the experimental value. With the Nusselt number calculated from the Dittus-Boelter correlation the agreement is even better, with a difference of less than 1%. Consequently, the small differences between the theoretical predictions and the experiment validate the evaluation of the total convective heat transfer based on water temperature measurements. In order to validate the evaluation of the term *A* based on the experimental measurements, a 2D axisymmetric numerical model was developed using the commercial CFD code Fluent. The computational domain corresponds to the total length of the pipe and simulations were carried out by using a constant mass flow rate as inlet condition, by specifying an operating temperature at the inlet of the *developing section* and by using a constant pressure at the outlet section. Boundary conditions were defined as the measured wall temperatures along the pipe. An incompressible turbulent model, using the Reynolds stress model of turbulence to account for the effects of streamline curvature, swirl, rotation, and rapid changes in strain rate, was solved. Simulation result for Q_{conv} is 472 W, i.e. a difference of around 4% with the experimental result, which verifies the

computation accuracy. Comparison between experimental and simulated results for the term *A* shows a difference of less than 3%. These agreements validate the determination of the terms in the energy balance equation (Eq. 10) in steady state operation using the experimental setup. Comparison between Q_{conv} and term *A* of Eq. 10, in the case of the steady turbulent flow, shows that the calculation of the variation of the time-averaged enthalpy of air is not sufficient to correctly compute the total time-averaged convective heat transfer: not taking into account the turbulent term may lead to an underestimation of the total time-averaged convective heat transfer of around 15%.

It is observed from Fig. 5 that the difference between Q_{conv} and term *A* shows a significant variation as a function of the pulsation frequency: the values of Q_{conv} can be higher (grey zone) than, equal to or lower (red zone) than the term *A*. Assuming that the turbulent term in Eq. 10 cannot be negative, which physically would represent a creation of turbulent heat flux inside the test-section, it can be concluded that a negative value of the term $\{\overline{\tilde{u}\tilde{T}}\}_{\Sigma}\Big|_0^L$ may occur. It is of interest to note that a negative value of term *B* (for instance for a pulsation frequency of 80 Hz) describes an energy contribution to the control volume, through the outlet section, due to the pulsating component of the flow. This mechanism is experimentally made possible by the combination of a warming of the air, once it has left the test-section, followed by a flow reversal. Downstream the test-section, the steel pipe was not water cooled and the experimental measurements showed that, after the test-section outlet, the air near the wall had a lower temperature than the external wall of the pipe. Moreover, the calculation of the particle displacement from the instantaneous air velocity profile showed that, when a flow reversal occurs, the air passes through the boundaries of the test-section several times. To experimentally demonstrate the importance of this mechanism, the steel pipe downstream the test-section was cooled by using dry ice in contact with the external wall of the pipe. Dry ice is in solid state at a temperature of -78.5°C and, once subjected to the ambient conditions, it sublimates, absorbing energy from the ambient to ensure the phase change. In this manner, it was possible to impose an external wall temperature of around -40°C for all the experiments. In these conditions, the results for Q_{conv} and term *A* are shown in Fig. 6. For each of the pulsation frequencies investigated, it can be observed, on the one hand, that Q_{conv} is always higher than the variation of the time-averaged air enthalpy and, on the other hand, that Q_{conv} exchanged during the use of dry ice is also always higher than that without dry ice (see Fig. 5). As a consequence, these results show that, in the present experimental configuration, an energy contribution coming from the ambient downstream the test-section can occur in the case of reversing pulsating flows.

4.3. Time-averaged heat transfer calculation and analysis

The time-averaged Nusselt number $Nu = h_{air}D/\lambda$ was evaluated by modelling the heat transfer between the hot air and the water with three thermal resistances placed in series to describe the internal forced convection of the air, the radial conduction through the wall and the forced convection of the water. The air convective heat transfer coefficient h_{air} assumes the following form:

$$h_{air} = \left[2\pi\, R_{in}\, L \left(\frac{\Delta T_{lm}}{Q_{conv}} - \frac{\ln(R_{out}/R_{in})}{2\pi\, L\, \lambda_{wall}} - \frac{1}{h_{water}\, 2\pi\, R_{out}\, L}\right)\right]^{-1} \quad (12)$$

where R_{in} and R_{out} are the inner and outer radii of the annular section of the pipe, L is the length of the test-section, λ_{wall} is the thermal conductivity of the wall, ΔT_{lm} is the logarithmic temperature difference usually used in the case of heat exchangers and h_{water} is the convective heat transfer coefficient of the water. The latter was calculated according to Rohsenow et al. [25] with a Nusselt number of 4.4, and ΔT_{lm} was calculated according to the following equation [26]:

$$\Delta T_{lm} = \frac{\left(T_{b_{in}} - T_{H2O-in}\right) - \left(T_{b_{out}} - T_{H2O-out}\right)}{\ln\left(T_{b_{in}} - T_{H2O-in}\right) - \ln\left(T_{b_{out}} - T_{H2O-out}\right)} \quad (13)$$

where $T_{b_{in}}$ and $T_{b_{out}}$ are respectively the input and output bulk temperatures of the air, calculated as the surface integral of the four measured temperatures. $T_{H2O-out}$ and T_{H2O-in} are the outlet and inlet water temperatures. The relative time-averaged Nusselt number (defined as the ratio of the time-averaged Nusselt number for the pulsating flow to the corresponding one for a steady flow with the same time-averaged Reynolds number), Nu_{rel}, is reported on Fig. 7. Results show that, for the entire frequency range, the relative time-averaged Nusselt number is always greater than 1: flow pulsation has a positive effect on heat transfers so that an enhancement of the internal forced convection, in comparison to the steady flow, is observed. Cooling the pipe downstream the test section only adds a positive offset to the relative time-averaged Nusselt number on the entire frequency range, without modifying the finding of the heat transfer enhancement. This offset is due to the increase in Q_{conv} because of the increase in the heat energy advection by the oscillating component of the flow. It can also be observed that, at the frequencies of 22.5, 50 and 80 Hz, a local maximum of the relative time-averaged Nusselt number appears. Thanks to the previous acoustic characterization of the system, it is possible to identify these frequencies as the 2nd, 3rd and 4th resonance modes of the system (see Table 1). Similar results were found by varying the pipe length for this time-averaged Reynolds number: for each of the pipe lengths tested when the flow is excited, with a pulsation frequency equal to one of the resonance modes, a heat transfer enhancement occurs. However, the magnitude of the heat transfer enhancement differs for each resonance mode and pipe length. This kind of result suggests that a coherent heat transfer enhancement mechanism exists when the flow is in resonant state.

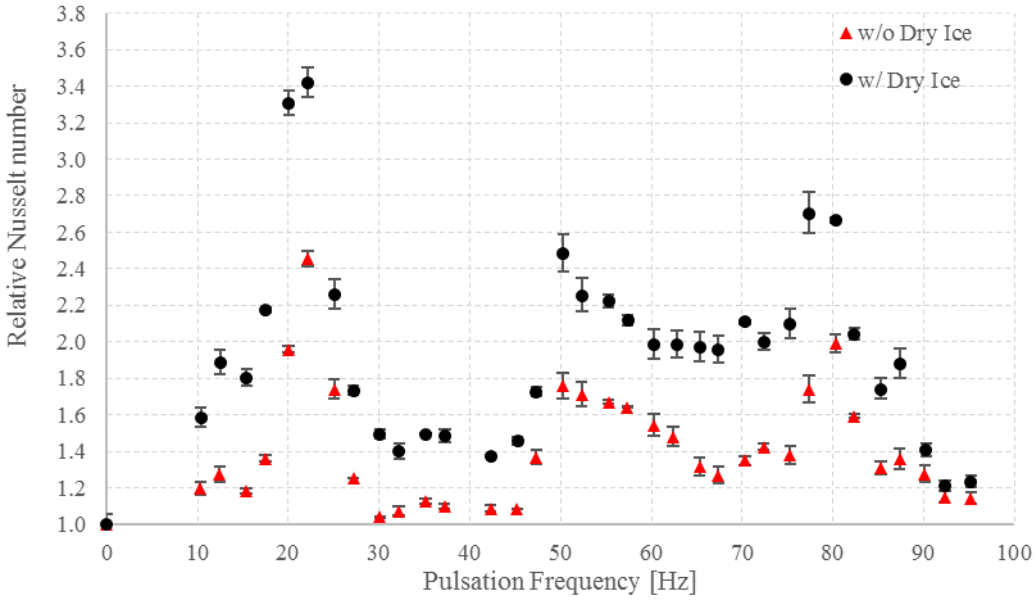

Figure 7: Relative time-averaged Nusselt number, L = 5.91m

In order to describe the mechanism of resonance and to investigate the phenomenon of heat transfer enhancement, the instantaneous measurements of the radial profile of the air velocity and of the static pressure at the middle of the test-section (section B – B' in Fig. 2) were analyzed. The phase-averaged axial component of the air velocity and the phase-averaged air static pressure are shown in Figs. 8 and 9. Two particular frequencies of 10 and 22.5 Hz have been chosen. It can be observed that at 22.5 Hz, which corresponds to the 2nd resonance mode, the amplitudes of velocity and pressure pulsations increase in comparison with the 10 Hz case: this is the consequence of the system acoustic resonance. The pulsation source excites the system with a mass injection that has a frequency equal to the system resonance mode (characterized and shown in the previous section). At this frequency, the response of the system to sound waves becomes very large. Such acoustic resonance, characteristic of the pressure field in the pipe, is transferred to the velocity field, as the phase-averaged velocity shows. Results also show that flow reversals appear for both frequencies and that the pulsation amplitude of the velocity variation is proportional to the pressure pulsation amplitude, in accordance with the acoustic linear theory for incompressible flows. It can also be noted that the instantaneous profiles do not have a sinusoidal waveform, because of the system cannot be assumed to behave as an open-end pipe due to the presence of the outlet plenum that modifies the reflection of the acoustic waves once they reach the end of the straight pipe. Although the pressure and velocity profiles are not in agreement with the quarter-wave-tube resonance, a phase delay (different from 45° for the case of a theoretical open-end pipe) between the maximum points of the air velocity and of the pressure exists.

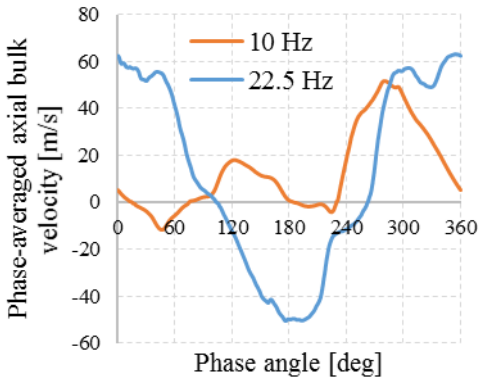

Figure 8: Axial component of the phase-averaged bulk air velocity, axial position B-B', L = 5.91m, Re = 30000

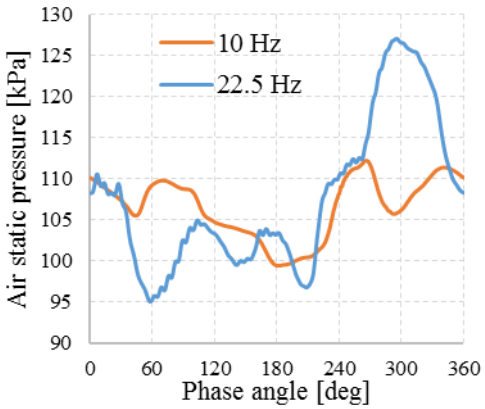

Figure 9: Phase-averaged air static pressure, axial position B-B', L = 5.91m, Re = 30000

Using the radial instantaneous profiles of the axial velocity and of the temperature, it is possible to calculate the local values of the terms which spatial derivatives appear in Eq. 9. In order to be in agreement with the 1D approach, the physical quantities correspond to the integral of the measured profiles on the cross section. As previously reported, the wall cooling by dry ice does not change the main finding on the heat transfer enhancement. For this reason, in the remaining part of the paper, only the results for the experimental conditions corresponding to the case without the pipe cooling by dry ice have been reported. Instantaneous measurements were conducted only for pulsation frequencies below 30 Hz since the size of the thermocouple implies that measurements for higher frequencies cannot be exploited due to the time constant of the thermocouple that cannot be compensated using a Kalman filter method. The measurement procedure of the instantaneous profiles of air axial velocity, using hot-wire anemometry, and air temperature, with micro unsheathed thermocouples, requires a correction of the hot-wire signals to account for the temperature variation of air as well as a thermocouple signal compensation for the sensor time delay. For frequencies higher than 30 Hz, the implicit filtering of the real temperature variations, due to the thermal inertia of the sensors, makes compensation of the thermocouple signal unfeasible, nor does it allow temperature compensation of the hot-wire signal. The pulsation frequencies below 30 Hz were chosen as a function of particular heat transfer conditions: 10 Hz and 12.5 Hz were selected for the light impact on heat transfers, 20 Hz and 22.5 Hz because of their vicinity to the second resonance mode of the pipe, and 30 Hz because it has the smallest relative Nusselt number. Results for the terms $\{\widetilde{\tilde{u}\tilde{T}}\}_{\Sigma}$ and $\Delta< u >/\bar{u}$ are reported in Fig. 10 and Fig. 11.

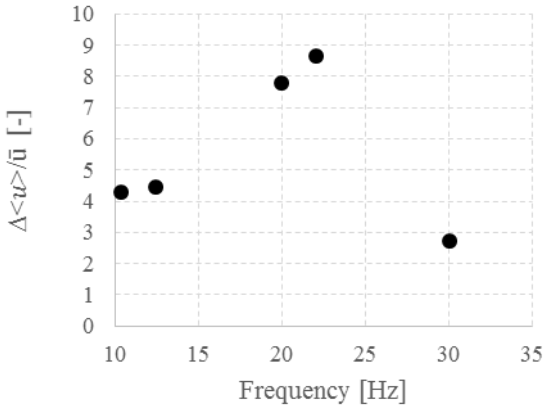

Figure 10: $\Delta< u >/\bar{u}$ *as a function of the pulsation frequency*

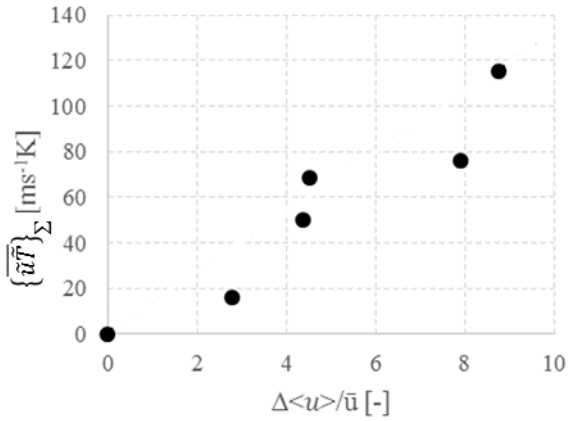

Figure 11: $\{\overline{\tilde{u}\tilde{T}}\}_{\Sigma}$ *as a function of* $\Delta< u >/\bar{u}$

$\Delta< u >/\bar{u}$ represents the weight of the phase-averaged velocity oscillation amplitude on the time-averaged velocity component and characterizes the increase in the oscillating component of the flow due to pulsation. Results in Fig. 10 show a maximum of the term $\Delta< u >/\bar{u}$ corresponding to the resonance frequency of the system, indicating that a flow resonance implies a wide oscillating component of the velocity. Furthermore since $\Delta< u >/\bar{u}$ values are all higher than 1, it can be concluded that flow reversal occurs for all the frequencies analyzed in Fig. 10, as confirmed by the instantaneous measurements of the air velocity with the double wire probe. Results in Fig. 11 show the term $\{\overline{\tilde{u}\tilde{T}}\}_{\Sigma}$ as a function of $\Delta< u >/\bar{u}$. By linking Figs. 10 and 11 it can be observed that large velocity oscillations, which correspond to high $\Delta< u >/\bar{u}$ values, are favored for pulsation frequencies close to the resonance frequency (the highest values of $\Delta< u >/\bar{u}$ correspond to the frequencies around 22.5 Hz, i.e. the second resonance mode of the system) and lead to an increase of $\{\overline{\tilde{u}\tilde{T}}\}_{\Sigma}$ as a function of $\Delta< u >/\bar{u}$. Trend analysis observed on Fig. 11 can be performed, under the assumption that the axial velocity is constant inside a given cross section, by considering only the first harmonics of the oscillating components of the velocity and temperature profiles, which represent the biggest structures in the velocity and temperature fields containing the major part of the kinetic and thermal energies:

$$\tilde{u} = \Delta< u > \sin(\omega t)\,, \qquad \tilde{T} = \Delta< T > \sin(\omega t + \varphi) \tag{14}$$

From the definition of $\{\overline{\tilde{u}\tilde{T}}\}_{\Sigma}$, it can be written:

$$\{\overline{\tilde{u}\tilde{T}}\}_{\Sigma} = \Delta< u > \Delta< T > \int_{period} \sin(\omega t)\sin(\omega t + \varphi)\; dt \tag{15}$$

In the right-hand side of Eq. 15, the integral over a cycle period assumes a definite constant value, which leads to a proportionality of $\{\overline{\tilde{u}\tilde{T}}\}_{\Sigma}$ with the product $\Delta< u > \Delta< T >$. Due to the complex turbulent pulsating problem, it is not possible to propose an exact analytical solution for $\Delta< u >$ and $\Delta< T >$. Nevertheless, according to the analytical development proposed for a pulsating laminar pipe flow by Fagri et al. [27], it can be assumed, using a first-order approximation in ω, that

$\Delta< T >$ is proportional to the amplitude of the velocity oscillations. According to Eq. 14, $\{\overline{\tilde{u}\tilde{T}}\}_{\Sigma}$ is then also found proportional to the amplitude of the velocity oscillations $\Delta< u >$ in a quadratic form when only the biggest structures of the flow are considered. As the time-averaged velocity component $\bar{u}$ is constant for all experiments, the experimental results reported on Fig. 11 seem to be consistent with this monotonic trend. As a conclusion of this analysis, the heat transfer enhancement for these frequencies, observed on Fig. 7, is therefore mainly attributed to a large oscillating component of the fluid velocity which increases the oscillating heat advection.

In order to characterize the impact of the pulsation frequency on the turbulent energy advection, the term *C* in Eq. 10 should be evaluated by measurements of the instantaneous radial profiles of air velocity and temperature. Although hot-wires have a bandwidth frequency up to 10 kHz, which is high enough to measure the turbulent variation of the air velocity, the thermocouples are not adapted to measure turbulent temperature fluctuations because of their long response time. Consequently, the term $\{\overline{< u'T' >}\}_{\Sigma}$ cannot be computed relevantly from the instantaneous experimental measurements. By exploiting the Reynolds analogy between momentum and heat transport equations, these limitations may be overcome. From the 2D momentum balance equation for an incompressible pulsating turbulent pipe flow, in which the phase and time averaging operators are applied, the following equation is obtained:

$$\rho\left(\underbrace{\frac{\partial\{\bar{u}\bar{u}\}_{\Sigma}}{\partial x}}_{\hat{A}}+\underbrace{\frac{\partial\{\bar{\tilde{u}}\bar{\tilde{u}}\}_{\Sigma}}{\partial x}}_{\hat{B}}+\underbrace{\frac{\partial\{\overline{< u'u' >}\}_{\Sigma}}{\partial x}}_{\hat{C}}\right)=\mu\left(\underbrace{\frac{\partial^2\{\bar{u}\}_{\Sigma}}{\partial x^2}}_{\hat{D}}\right)+\underbrace{\frac{\partial\bar{p}}{\partial x}}_{\hat{E}} \tag{16}$$

It can be observed that the terms *A*, *B* and *C*, which correspond to the different components of the axial momentum of the flow, have the same mathematical form as the 3 terms in the left-hand side of Eq. 9 and differ only from these terms by a multiplicative coefficient which corresponds to the Prandtl number. The terms *D* and *E* correspond, respectively, to the viscous dissipation and to the pressure losses due to the viscous effect with the wall of the pipe. For a turbulent flow with a Prandtl number around 1, which means that the diffusion of momentum and thermal energy is similar, the Reynolds analogy implies that if a given flow field can be determined, the heat transfer characteristics can be found. In the experimental configuration of this work, the Prandtl number is about 0.69 (and is slightly dependent on temperature) so that the Reynolds analogy is commonly adopted in these conditions. Consequently, the terms in the left-hand side of Eq. 9 and Eq. 16 must exhibit a similar behavior. However, the limitations of the velocity and temperature measurements mean that the terms in Eq. 16 cannot be computed directly from the experimental measurements for a hot turbulent pulsating flow. Since the hot-wire signal compensation for the temperature effect was applied only to the phase-averaged signals it was not possible to extract the turbulent component of the air axial velocity from hot-wire signals. To overcome these measurement limitations, experiments were conducted for a cold turbulent pulsating flow. Considering temperature as a passive scalar field transported by the turbulent flow, it can be assumed that a cold pulsating flow has a velocity field behavior similar to that of a hot pulsating flow with the same time-averaged Reynolds number. The same time-averaged Reynolds number implies that the time-averaged

467 turbulent contribution to the momentum transport should be the same in hot and cold flow conditions. Using these assumptions,
468 experiments were conducted for a pulsating turbulent pipe flow with a centerline time-averaged temperature of 25°C. In these
469 experimental conditions, temperature variations due to the flow compression are negligible and do not disturb the hot-wire
470 signal. Consequently, instantaneous hot-wire signals were not compensated for the temperature impact, and were directly
471 decomposed according to Eq. 3 to allow the calculation of the turbulent component of the air axial velocity. To account for the
472 decrease in the sound velocity because of the decrease in the flow temperature, the total pipe length was reduced so as to have
473 the same resonance frequencies for the cold pulsating flow as for the hot pulsating flow. The computed terms *A*, *B* and *C* of
474 Eq. 16 are reported in Table 2. Results show that in the case of resonant flow the time-averaged product of the oscillating
475 component of the air axial velocity $\{\widetilde{\bar{u}}\widetilde{\bar{u}}\}_{\sum}$ increases. This behavior is in agreement with the variation of the term $\overline{\{\tilde{u}\tilde{T}\}_{\sum}}$, as
476 previously shown. The turbulent term $\left\{\overline{< u'u' >}\right\}_{\sum}$ also shows a local maximum corresponding to the fluid resonant state,
477 suggesting that pulsation frequency impacts the turbulent properties of the flow. Nevertheless, because of its lower order of
478 magnitude than the term $\{\widetilde{\bar{u}}\widetilde{\bar{u}}\}_{\sum}$, its contribution to the momentum transport equation can be neglected in comparison to that
479 of the term $\{\widetilde{\bar{u}}\widetilde{\bar{u}}\}_{\sum}$. These results can be similarly applied to the heat flux transport equation: the oscillating heat flux advection
480 plays the main role in the convective heat transfer enhancement compared to the effect of the turbulent heat flux advection on
481 heat transfer.

Frequency [Hz]	$\{\bar{u}\bar{u}\}_{\sum}$ **[m²/s²]**	$\{\widetilde{\bar{u}}\widetilde{\bar{u}}\}_{\sum}$ **[m²/s²]**	$\{< u'u' >\}_{\sum}$ **[m²/s²]**
10.4	245.7	375.8	6.4
12.4	242.3	293.4	3.6
20.0	211.3	1291.8	22.1
22.1	231.3	1893.5	40.3
30.0	214.6	210.2	2.6

482 *Table 2 : Terms A, B, C of Eq. 16*

483 ***4.4. Towards a Nusselt correlation for pulsating turbulent pipe flows***

484 The quasi-steady assumption is generally adopted to solve analytically or numerically the heat transfer problem for a pulsating
485 flow. Due to the fact that the flow is assumed to behave as if it were steady at the instantaneous velocity, the instantaneous
486 local heat transfer is assumed to balance the variation of the fluid local properties at any time in the cycle. However, this
487 assumption implies that the flow reaches a fully developed equilibrium within a time much less than the cycle time and is thus
488 only valid for flows with low frequencies or small oscillation amplitudes. Fig. 12 shows, for three frequencies, the velocity
489 boundary layer thickness δ, calculated according Eq. 17 and nondimensionalized by the pipe radius.

$$\delta = \int_0^{R_{in}} \left(1 - \frac{< u_r >}{< u_{centerline} >}\right) dr \qquad (17)$$

where $< u_r >$ represents the axial component of the phase-averaged air velocity, which is function of the distance from the wall. It is shown that the dimensionless velocity boundary layer thickness reaches a value of 1 for several phases. For these phase angles, $< u_{centerline} >$ is equal to zero and $< u_r > / < u_{centerline} >$ tends to infinity, which corresponds to flow reversal phases. Results also show that, for 10 Hz and 22.5 Hz, the velocity boundary layer thickness strongly fluctuates during the cycle. This is characteristic of flow structures that are not in equilibrium near the wall. As the thermal energy is transported by the velocity field, also the heat transfer is not in equilibrium. Consequently, the quasi-steady approach is not suitable for these two pulsation frequencies. With regard to the 30 Hz case, even if the quasi-steady assumption is still not valid, the fluctuation of the velocity boundary layer thickness is decreased compared to the two other frequencies.

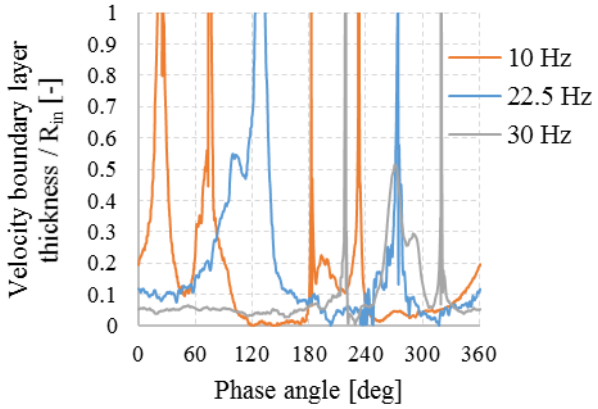

Figure 12: Velocity boundary layer thickness on the pipe internal radius, axial position B-B', L = 5.91m, Re = 30000

Whereas for a stationary turbulent pipe flow it has been largely demonstrated that the Nusselt number is a function of the Gz_T, Re and Pr numbers, for an unsteady convection process the Vaschy-Buckingham Π analysis applied in low-speed laminar flow conditions in a pipe shows that the time-averaged Nusselt number may depend on as many as seven dimensionless parameters [28]. Nevertheless, some of these parameters are not affected by the flow pulsation variation. As the time-averaged mass flow rate was kept constant for all experiments, the time-averaged Reynolds number is considered constant. In the same way, the Prandtl number for the air is slightly impacted by the temperature variations and is here assumed constant. The Graetz number, defined as $Gz_T = D/L_d RePr$, is useful in determining the thermally developing flow entrance length L_d for the description of entrance effects on laminar flow heat transfer. As it is applicable mainly to transient heat conduction in a laminar pipe flow, Gz_T is not a relevant parameter in this study, where the flow is in turbulent conditions, to describe the pulsation effect on heat transfer. Acoustic streaming, characterized by the parameter $U_0/\omega D$, is described by Jackson et al. [29] as a phenomenon that appears in resonant pulsating flows and generates a secondary time-averaged velocity component. The flow generated by acoustic streaming is characterized by large longitudinal counter-rotating vortices that are one quarter the length of the acoustic wavelength and occur at half-wavelength intervals. In the quarter wavelength between these vortical structures, acoustic streaming causes a velocity component towards the wall of the pipe, increasing the velocity near the wall. As shown by Lei et al. [30], axial velocity increases rapidly from zero at the wall to the maximum at the thickness of the acoustic layer

and decreases slowly with the further increase of the distance from the wall. Stagnation points, corresponding to a node, are located at equally spaced intervals equal to one quarter of the pressure wavelength. In the present study, the flow was not always in resonant state, which means that acoustic streaming was not generated at all the investigated pulsation frequencies. When the flow was excited at a pulsation frequency equals to one of the resonant mode frequencies, e.g. 22.5 Hz, experimental profiles of the time-averaged axial component of the air velocity were analyzed using the hot-wire anemometer measurements. As the velocity profiles were measured at a fixed axial position of the test section (see Fig. 2), it was verified that this position was not located on a node of the acoustic wave (at the pulsation frequency of 22.5 Hz, assuming a time-averaged temperature of 150°C, the pressure wavelength assumes a value of about 18.3 m). Experimental profiles of the time-averaged axial component of the air velocity showed that the axial velocity was always positive. This means that no recirculation cell was formed in flow resonant state and that the acoustic streaming effect can be neglected in the Nusselt number correlation analysis. In Fig. 13, the relative spatial and time-averaged Nusselt number is plotted versus the remaining relevant parameters: the grouping $c/\omega D$, which is a measure of the wavelength of the applied pressure oscillation to the relevant streamwise length scale (c is the velocity of sound) ; the Womersley number, defined as $Wo = (D/2)\sqrt{\rho\omega/\mu}$, which is a ratio of the channel height to the Stokes boundary-layer thickness, is a dimensionless expression of the pulsatile flow frequency in relation to viscous effects ; the amplitude ratio $\Delta< u >/\bar{u}$, which is a measure of the amplitude of the velocity waveform. These parameters are calculated from the experiments for all the investigated pulsation frequencies lower than 30 Hz. As previously stated, results were computed for the experiments without pipe cooling by dry ice.

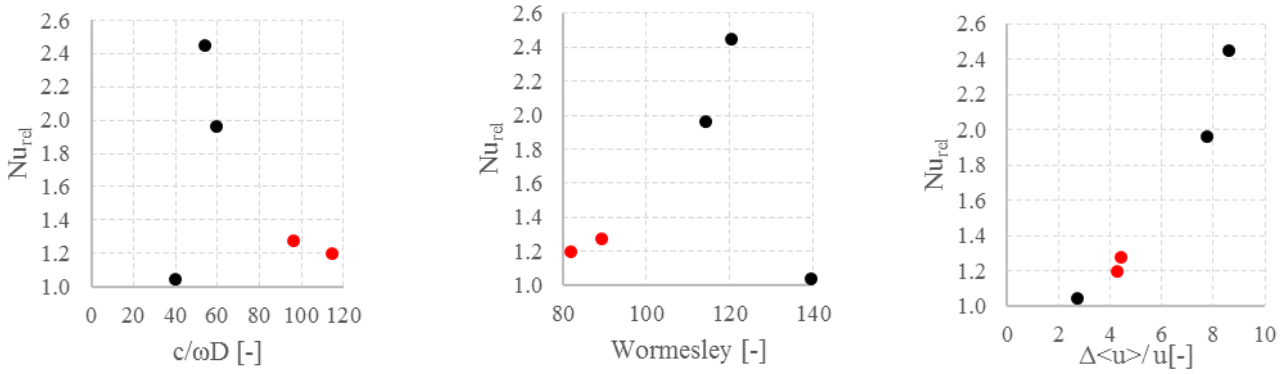

(a) Nu_{rel} vs $c/\omega D$ *(b) Nu_{rel} vs Wo* *(c) Nu_{rel} vs $\Delta< u >/\bar{u}$*

Figure 13: Relative time-averaged Nusselt number as a function of dimensionless parameters

The results in Fig. 13a show the dependence of the relative Nusselt number on the term $c/\omega D$: an increase in the pulsation frequency (corresponding to a decrease in $c/\omega D$ since the speed of sound can be considered constant, as the air temperature at the inlet of the test-section is maintained constant for all experiments) leads to an increase in Nu_{rel} till a maximum corresponding to the second resonance mode frequency. This local maximum is followed by a decrease in the heat transfer enhancement when the pulsation frequency is increased. In Fig. 13b, Nu_{rel} is plotted versus the Womersley number. According to the definitions of the Womersley number and of the Stokes layer, an increase in the pulsation frequency leads to a thinning

of the viscous fluid boundary layer for a pulsating flow, which means that the velocity field is affected in a more restricted zone near the wall with the increase in *Wo*. However, in terms of heat transfer enhancement, an optimal value of the Womersley number exists for the maximization of the relative Nusselt number. This result indicates that the transport of energy and the transport of the momentum are differently impacted by the variation of the Womersley number. This result agrees with the experimental results in Ref. [31], where a local maximum in the heat transfer enhancement was found for a particular value of *Wo*. In the present study, this optimal value of *Wo* corresponds to a pulsation frequency identified as a resonance frequency of the system (the second resonance mode). The monotonic dependence of the relative Nusselt number on velocity amplitude ratio $\Delta< u >/\bar{u}$ is shown in Fig. 13c. For a constant time-averaged velocity, the relative Nusselt number increases with the velocity oscillation amplitude. When the velocity oscillation amplitude is relatively low (for an amplitude ratio roughly less than 4), the heat transfer is moderately enhanced, while Nu_{rel} increases rapidly when $\Delta< u >/\bar{u} > 4$. A similar behavior was found by Wang et al. [32] in their numerical study. Fig. 13c also shows that relatively constant values of Nu_{rel} are obtained for relatively constant values of $\Delta< u >/\bar{u}$, as depicted by the red markers. Results corresponding to these two same experiments are also marked by the red points on Figs. 13a and 13b, and it can be noted that a slight variation in the relative Nusselt number corresponds to significant variations in $c/\omega D$ and of *Wo*. These results are consistent with the developed analytical formulation combined with the experimental measurements that have shown that a large oscillating velocity component is the most important mechanism in the heat transfer enhancement. This mechanism is described by the amplitude of the velocity waveform and, consequently, the characteristic term that should primarily be taken into account in a correlation to predict heat transfers in the case of a pulsating flow is $\Delta< u >/\bar{u}$. Nevertheless, even if Fig. 11 has shown that this term is directly linked to the oscillating heat flux advection, this approach does not identify the physical mechanisms involved in the heat transfer enhancement. This velocity waveform parameter is representative of the adopted 1D approach that does not quantify the energy transport mechanisms in the radial direction that are integrated into the average over the cross section. For $\Delta< u >/\bar{u}$ values higher than 1, a periodic flow reversal initiates downstream and rapidly propagates upstream. As reversed fluid moves upstream, it encounters forward-moving fluid and a radial velocity must be established to preserve continuity. The occurrence of these mass ejections may increase the radial transport of energy and should be evidenced with a 2D analysis.

5. CONCLUSIONS

The results of an experimental investigation of convective heat transfer in pulsating turbulent flow in a pipe, with large-amplitude oscillations, have been reported. The experimental apparatus was designed to generate a turbulent pulsating hot air flow representative of engine exhaust flow conditions. Particular attention was paid to the calculation of the time-averaged convective heat transfer by developing a 1D analytical formulation of the heat transfer problem for a pulsating turbulent pipe flow. This development evidenced that whenever a direct measurement of the total time-averaged convective heat transfer is not available, instantaneous measurements of the air velocity and temperature are required to correctly compute the terms

linked to the oscillating component of the flow in the energy balance equation. Experimental results showed that, in the case of a reversed pulsating flow, a contribution to the energy balance equation through the boundaries, which impacts the total convective heat transfers, may occur. Flow pulsation was found to enhance heat transfers in the entire range of frequencies investigated. In particular, it was experimentally observed that, when the flow is excited with a frequency equal to a resonance mode of the system, a strong increase in heat transfers occurs. Instantaneous measurements of air velocity and temperature demonstrated that the increase in the energy axial advection due to the oscillating component of the velocity is the major cause of the heat transfer enhancement. This behavior was observed to be independent of the pipe length, and therefore independent of the acoustic resonance modes of the pipe. These results suggest that flow pulsation may be used as an active method for heat transfer enhancement. The relative Nusselt number was found to be directly linked to the ratio between the velocity oscillation amplitude and the velocity time-averaged component, suggesting that this parameter is representative of the predominant heat transfer enhancement mechanism and should be included in a convective coefficient correlation for the modeling of heat transfers, not only in engine exhaust systems but also for all engineering applications where heat is transferred under pulsating conditions.

ACKNOWLEDGEMENTS

This work was supported by the 'OpenLab Energetics' program, thanks to the partnership between the Groupe PSA and the PRISME Laboratory of the University of Orléans.

REFERENCES

[1] R. Host, P. Moilanen, M. Fried, B. Bogi, Exhaust System Thermal Management : A Process to Optimize Exhaust Enthalpy for Cold Start Emissions Reduction, SAE Tech. Pap. (2017).

[2] C. Sprouse III, C. Depcik, Review of organic Rankine cycles for internal combustion engine exhaust waste heat recovery, Appl. Therm. Eng. 51 (2013) 711–722.

[3] J.E. Dec, J.O. Keller, Pulse combustor tail-pipe heat-transfer dependence on frequency, amplitude, and mean flow rate, Combust. Flame. 77 (1989) 359–374.

[4] J.E. Dec, J.O. Keller, V.S. Arpaci, Heat transfer enhancement in the oscillating turbulent flow of a pulse combustor tail pipe, Int. J. Heat Mass Transf. 35 (1992) 2311–2325.

[5] J.E. Dec, J.O. Keller, Time-resolved Gas Temperatures in the Oscillating Turbulent Flow of a Pulse Combustor Tail Pipe, Combust. Flame. 80 (1990) 358–370.

[6] J.E. Dec, J.O. Keller, I. Hongo, Time-Resolved Velocities and Turbulence in the Oscillating Flow of a Pulse Combustor Tail Pipe, Combust. Flame. 83 (1991) 271–292.

[7] Y. Xu, M. Zhai, L. Guo, P. Dong, J. Chen, Z. Wang, Characteristics of the pulsating flow and heat transfer in an elbow tailpipe of a self-excited Helmholtz pulse combustor, Appl. Therm. Eng. 108 (2016) 567–580.

[8] M. Zhai, X. Wang, T. Ge, Y. Zhang, P. Dong, F. Wang, G. Liu, Y. Huang, Heat transfer in valveless Helmholtz pulse combustor straight and elbow tailpipes, Int. J. Heat Mass Transf. 91 (2015) 1018–1025.

[9] J.T. Patel, M.H. Attal, An Experimental Investigation of Heat Transfer Characteristics of Pulsating Flow in Pipe, Int. J. Curr. Eng. Technol. 6 (2016) 1515–1521.

[10] A.E. Zohir, Heat Transfer Characteristics in a Heat Exchanger for Turbulent Pulsating Water Flow with Different Amplitudes, J. Am. Sci. 8 (2012) 241–250.

[11] S.A.M. Said, Al-Farayedhi A., M. Habib, S.A. Gbadebo, A. Asghar, S. Al-Dini, Experimental Investigation of Heat Transfer in Pulsating Turbulent Pipe Flow, J. Heat Fluid Flow. (2005) 54.

[12] S.V. Nishandar, R.H. Yadav, Experimental investigation of heat transfer characteristics of pulsating turbulent flow in a pipe, Int. Res. J. Eng. Technol. 2 (2015) 487–492.

[13] E.A.M. Elshafei, Safwat Mohamed, H. Mansour, M. Sakr, Numerical study of heat transfer in pulsating turbulent air flow, J. Eng. Technol. Res. 4 (2012) 89–97.

[14] H.R. Kharvani, F.I. Doshmanziari, A.E. Zohir, D. Jalali-Vahid, An experimental investigation of heat transfer in a spiral-coil tube with pulsating turbulent water flow, Heat Mass Transf. (2015).

[15] H. Ghaedamini, P.S. Lee, C.J. Teo, Enhanced transport phenomenon in small scales using chaotic advection near resonance, Int. J. Heat Mass Transf. 77 (2014) 802–808

[16] C. Wantha, Effect and heat transfer correlations of finned tube heat exchanger under unsteady pulsating flows, Int. J. Heat Mass Transf. 99 (2016) 141–148.

[17] Z. Guo, H.J. Sung, Analysis of the Nusselt number in pulsating pipe flow, Int. J. Heat Mass Transf. 40 (1997) 2486–2489.

[18] C. Guardiola, P. Olmeda, B. Pla, P. Bares, In-cylinder pressure based model for exhaust temperature estimation in internal combustion engines, Appl. Therm. Eng. 115 (2017) 212–220.

[19] J.M. Luján, H. Climent, P. Olmeda, V.D. Jiménez, Heat transfer modeling in exhaust systems of high-performance two-stroke engines, Appl. Therm. Eng. 69 (2014) 96–104.

[20] W.C. Reynolds, A.K.M.F. Hussain, The mechanics of an organized wave in turbulent shear flow. Part 3. Theoretical models and comparisons with experiments, J. Fluid Mech. 54 (1972) 263–288.

[21] R.E. Johnk, T.J. Hanratty, Temperature profiles for turbulent flow of air in a pipe: I, The fully developed heat-transfer region, Chem. Eng. Sci. 17 (1962) 867–879.

[22] K. Kar, S. Roberts, R. Stone, M. Oldfield, B. French, Instantaneous exhaust temperature measurements using thermocouple compensation techniques, SAE Tech. Pap. (2004) 169–190.

[23] M. Tagawa, K. Kato, Y. Ohta, Response compensation of fine-wire temperature sensors, Rev. Sci. Instrum. 76 (2005).

[24] J.H. Lienhard, A heat transfer Textbook, Third Edit, Phlogiston Press, 2008.

[25] W.M. Rohsenow, J.R. Hartnett, Young I. Cho, Handbook of Heat Transfers, Third Edit, McGraw-Hill, 1998.

[26] L. Angeles, Convective heat and mass transfer, (2013).

[27] M. Faghri, K. Javdani, A. Faghri, Heat transfer with laminar pulsating flow in a pipe, Lett. Heat Mass Transf. 6 (1979) 259–270.

[28] S.P. Kearney, A.M. Jacobi, R.P. Lucht, Time-Resolved Thermal Boundary-Layer Structure in a Pulsatile Reversing Channel Flow, J. Heat Transfer. 123 (2001) 655–664.

[29] T.W. Jackson, K.R. Purdy, Resonant Pulsating Flow and Convective Heat Transfer, J. Heat Transfer. (1965) 507–512.

[30] H. Lei, D. Henry, H. Benhadid, Acoustic force model for the fluid flow under standing waves, Appl. Acoust. 72 (2011) 754–759.

[31] H. Li, Y. Zhong, X. Zhang, K. Deng, H. Lin, L. Cai, Experimental Study of Convective Heat Transfer in Pulsating Air Flow inside Circular Pipe, Int. Conf. Power Eng. (2007) 880–885.

[32] X. Wang, N. Zhang, Numerical analysis of heat transfer in pulsating turbulent flow in a pipe, Int. J. Heat Mass Transf. 48 (2005) 3957–3970.